Eigenvalue separation and eigenmode analysis by matrix-filling Monte Carlo methods

Vito Vitali, Florent Chevallier, Alexis Jinaphanh, Patrick Blaise, Andrea Zoia

Version of Record: https://www.sciencedirect.com/science/article/pii/S0306454921004394
Manuscript_8a129b4bf9a33ad92f1ff668e532e9f9

Eigenvalue separation and eigenmode analysis by matrix-filling Monte Carlo methods

Vito Vitali[a], Florent Chevallier[a], Alexis Jinaphanh[a], Patrick Blaise[b], Andrea Zoia[a,*]

[a] *Université Paris-Saclay, CEA, Service d'études des réacteurs et de mathématiques appliquées, 91191, Gif-sur-Yvette, France*
[b] *DES/Scientific Division Energies, CEA Saclay*

Abstract

Matrix-filling Monte Carlo methods can be successfully used to estimate higher-order k- and α-eigenmodes and eigenvalues of the Boltzmann equation. A novel matrix-filling Monte Carlo approach has been recently developed in Tripoli-4 ® in order to solve the α-eigenvalue problem, as a complement to the standard fission matrix method. The behavior of the fundamental and higher-order eigenpairs in the presence of decoupling factors is illustrated through a few relevant homogeneous and heterogeneous numerical benchmarks, with special emphasis on eigenvalue separation. We then revisit a selected experiment carried out during the EPILOGUE program in the EOLE critical facility of CEA Cadarache. Using spectral analysis by Monte Carlo as a 'numerical experiment' might help, e.g., in conceiving a future campaign in a zero-power research reactor.

Keywords: Time eigenvalues, Monte Carlo, matrix, eigenvalue separation, eigenfunctions, EOLE reactor

1. Introduction

The spectral properties of the Boltzmann equations are intimately related to the behaviour of nuclear systems (Duderstadt and Martin, 1979). Experimental and numerical investigations have shown that configurations with a small k-eigenvalue separation have an enhanced probability to propagate instabilities, and thus display complex space-time patterns; this is to be contrasted to systems

*Corresponding author
Email address: andrea.zoia@cea.fr (Andrea Zoia)

with a large eigenvalue separation, which conversely behave as point-kinetics (Pázsit and Dykin, 2018). In this respect, a prominent parameter is the dominance ratio DR $= k_1/k_0$, defined as the ratio between the first and the fundamental k-eigenvalue. If DR is much smaller than one, the core is tightly coupled and the effect of a localized perturbation will rapidly affect the entire core; conversely, if DR is close to one the core is loosely coupled and a localized perturbation might induce unwanted unevenly distributed phenomena (Pázsit and Dykin, 2018). Eigenvalue separation is especially relevant for loosely-coupled nuclear systems, such as breeders having alternating regions of highly-enriched fuel and depleted blankets, or spent fuel pools and reprocessing sites. By virtue of its key role in understanding the system kinetics, and in particular the reactor response due to external perturbations and tilts, the k-eigenvalue separation has been extensively investigated (Rubinstein and Kroese, 2007; Ebert et al., 1974; Beckner and Rydin, 1975; Hashimoto et al., 1991; Nishina and Tokashiki, 1996; Kobayashi, 1998).

In this paper, we will show how matrix-filling Monte Carlo methods can be usefully adopted for such applications, through the calculation of higher-order k- and α-eigenmodes and eigenvalues. In Sec. 2, we will first briefly recall the fission matrix approach (Urbatsch, 1992; Carney et al., 2014), a matrix-filling Monte Carlo method used in order to estimate the elements of a finite-size matrix whose eigenvectors and eigenvalues converge to those of the k-eigenvalue problem in the limit of an infinite matrix size. A matrix-filling Monte Carlo method suitable for α-eigenvalue analysis has been recently introduced by Betzler and co-workers (Betzler et al., 2014, 2015, 2018), as a useful complement to k-eigenvalue analysis. By expanding on these ideas, improved approaches for α-eigenvalue analysis have been proposed (Vitali et al., 2019; Variansyah et al., 2020), and will be also recalled in Sec. 2.

In order to better grasp the physical meaning of the eigenvalue separation, which is traditionally formulated for the k-eigenvalue problems (Duderstadt and Martin, 1979), in this work we will extend the spectral analysis by Monte Carlo simulation to the case of α-eigenvalues. A few relevant applications will be analyzed and the discrepancies between the higher α- and k-higher-order eigenpairs will be illustrated in Sec. 3. The aim is to examine whether the two modal expansions may convey different information content, with special focus on the eigenvalue separation. In particular, we will examine how the fundamental and higher-order eigenpairs behave in the presence of decoupling effects: starting from (homogeneous or heterogeneous) tightly coupled reactor configurations, we will progressively increase either the system size or the spatial heterogene-

ity[1]. For this purpose, some simple benchmark configurations will be selected where these effects are exacerbated. The eigenvalue separation and the shape of the eigenfunctions will be then carefully examined and commented.

In Sec. 4, our analysis will be then extended to the EPILOGUE experiment, carried out in the EOLE critical facility of CEA Cadarache. The EPILOGUE experiment was aimed at exploring – among others – the effects of the presence of a water blade into the core with respect to the detector response. By building on the numerical findings obtained for the benchmark configurations, we will simulate with TRIPOLI-4® the EPILOGUE experiment and compare the effects of the water blades on the fundamental and higher-order eigenpairs of the k- and α-bases. Furthermore, we will use Monte Carlo simulation as a 'numerical experiment' in order to explore the effects of including additional water blades into the core, thus increasing the decoupling effect. Conclusions will be finally drawn in Sec. 5.

2. Spectral analysis of the transport operators

2.1. k-eigenvalue problem

The k-eigenvalue formulation is possibly the best-known formulation for criticality analysis (Duderstadt and Martin, 1979). Starting from the Boltzmann equation without external sources, a stationary solution is sought. In order to preserve the equilibrium between neutron loss and production, a factor k is introduced to artificially reduce ($k > 1$) or increase ($k < 1$) the fission contributions. Such hypotheses lead to the k-eigenvalue problem

$$\mathcal{M}\varphi_k = \frac{1}{k}\mathcal{F}\varphi_k, \tag{1}$$

where

$$\mathcal{M} = \mathbf{\Omega}\cdot\nabla + \Sigma_t - \int\int d\mathbf{\Omega}' dE' \Sigma_s(\mathbf{r}, \mathbf{\Omega}', E' \rightarrow \mathbf{\Omega}, E) \tag{2}$$

[1]The natural spatial scale in order to properly characterize the system size is the migration length, i.e., the typical crow-flight neutron displacement within a fission generation (Bell and Glasstone, 1970).

is the net disappearance operator,

$$\mathcal{F} = \mathcal{F}_p + \sum_j \frac{\chi_d^j(E)}{4\pi}\mathcal{F}_d^j \tag{3}$$

$$= \frac{\chi_p(\mathbf{r},E)}{4\pi}\iint d\mathbf{\Omega}'dE'\nu_p(E')\Sigma_f(\mathbf{r},E') + \sum_j \frac{\chi_d^j(E)}{4\pi}\iint d\mathbf{\Omega}'dE'\nu_{d,j}(E')\Sigma_f(\mathbf{r},E') \tag{4}$$

is the total fission operator and (k,φ_k) are the k-eigenpairs, with the eigenvalues k and the corresponding eigenmodes $\varphi_k(\mathbf{r},\mathbf{\Omega},E)$. From a physical point of view, the eigenvalue problem in Eq. (1) corresponds to following the evolution of neutrons through fission generations (Henry, 1964).

Under suitable (mild) assumptions, there exists a fundamental eigenvalue k_0, positive and simple such that $k_0 > |k_n|$ for $n > 0$, associated to the real and positive fundamental eigenfunction φ_{k_0} (Asahi, 1975; Velarde et al., 1977). The value k_0, also known as the multiplication factor, represents the ratio between the neutrons produced by fission events and the neutrons absorbed or leaked from the system within a generation.

2.2. α-eigenvalue problem

Although the k-eigenvalue formulation is very useful for quickly ascertaining whether the system is critical, sub- or super-critical, one might in general be interested also in determining the asymptotic reactor behaviour with respect to time (Duderstadt and Martin, 1979). For this purpose, the strategy is to introduce the separation of the phase-space variables, postulating an exponential time-evolution of the neutron flux and precursor concentration. According to these assumptions, the vector $\Psi = \{\varphi, c_1, \ldots, c_J\}^T$ (collecting the neutron flux φ and the precursor concentrations c_j for each family $j = 1, \cdots, J$) reads $\Psi(\mathbf{r},\mathbf{\Omega},E,t) = \Psi_\alpha(\mathbf{r},\mathbf{\Omega},E)e^{\alpha t}$. The resulting α-eigenvalue problem is thus obtained as

$$\mathcal{A}\Psi_\alpha = \alpha\mathcal{B}\Psi_\alpha, \tag{5}$$

where the operators $\mathcal{A}$ and $\mathcal{B}$ are respectively defined as

$$\mathcal{A} = \begin{pmatrix} \mathcal{F}_p - \mathcal{M} & \lambda_1\frac{\chi_d^1}{4\pi} & \cdots & \lambda_J\frac{\chi_d^J}{4\pi} \\ \mathcal{F}_d^1 & -\lambda_1 & \cdots & 0 \\ \vdots & \vdots & \ddots & \vdots \\ \mathcal{F}_d^J & 0 & \cdots & -\lambda_J \end{pmatrix}, \tag{6}$$

and

$$\mathcal{B} = \begin{pmatrix} \frac{1}{v} & 0 & \cdots & 0 \\ 0 & 1 & \cdots & 0 \\ \vdots & \vdots & \ddots & \vdots \\ 0 & 0 & \cdots & 1 \end{pmatrix}. \tag{7}$$

The fundamental eigenvalue α_0 physically represents the inverse of the asymptotic reactor period (including precursor contributions), and the associated fundamental eigenfunction φ_{α_0} represents the asymptotic particle distribution. The spectral properties of the full system (5), including precursor contributions, have recently attracted renewed attention, in view of the practical applications in reactor kinetics (Singh et al., 2011; Nauchi, 2013; Zoia et al., 2015; Betzler et al., 2018; Vitali et al., 2019; Variansyah et al., 2020; Nauchi et al., 2020; Filiciotto et al., 2020).

Contrary to the k-eigenvalue formulation, the delay of fission neutrons emitted from precursor decay is explicitly taken into account, and the distributions for precursor concentrations are additional unknowns for Eq. (5). It is possible to recast Eq. (5) as an eigenvalue problem for the neutron flux alone by formally solving the precursor distribution as

$$c_\alpha^j = \frac{1}{\lambda_j + \alpha} \mathcal{F}_d^j \varphi_\alpha, \tag{8}$$

and substituting this formulation in the neutron equation. A new operator for the fission events is then defined as

$$\mathcal{F}_\alpha = \mathcal{F}_p + \sum_j \frac{\lambda_j}{\lambda_j + \alpha} \frac{\chi_d^j}{4\pi} \mathcal{F}_d^j, \tag{9}$$

which yields

$$[\mathcal{F}_\alpha - \mathcal{M}]\varphi_\alpha = \alpha \mathcal{B} \varphi_\alpha. \tag{10}$$

Equation (10) is now non-linear with respect to the eigenvalues (Weinberg, 1952).

The α-spectrum splits into a 'prompt' portion and a 'delayed' portion, which are easily distinguished on the complex plane (Sanchez and Tomatis, 2019). Numerical investigations have shown that the delayed part of the α spectrum consists of J 'clusters' of real eigenvalues, with the j-th cluster, $j = 1, \cdots, J$, being a countable set of eigenvalues in the interval $(-\lambda_j, -\lambda_{j-1})$, J being the total number of precursor families (we set λ_0 to infinity, by following the notation of (Sanchez and Tomatis, 2019)). These eigenvalues are tightly regrouped at the right of each decay constant $-\lambda_j$ for family j on the complex plane (Kaper, 1967; Foulke and

Gyftopoulos, 1967). The prompt part of the α-spectrum contains discrete eigenvalues, these latter appearing at the left of $-\lambda_J$ (Asahi, 1975) and a continuum portion (if any) at the left of the Corngold limit (Corngold, 1964). Figure 1 shows a typical spectrum of the first α-eigenvalues along the real axis for a super-critical system.

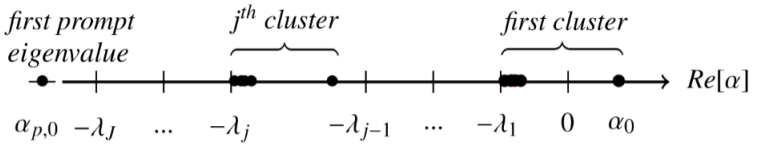

Figure 1: Typical spectrum of α-eigenvalues for a super-critical system. Sketch inspired by the reference (Sanchez and Tomatis, 2019).

2.3. Eigenvalue separation

The tightness of a reactor core is typically characterized in terms of the eigenvalue separation, which for the k-eigenvalue formulation reads

$$\text{E.S.}_n(k) = \frac{1}{k_n} - \frac{1}{k_0}, \tag{11}$$

with $n \geq 1$ (Pázsit and Dykin, 2018). The system is said to be *tightly coupled* if the first two eigenvalues are separated, and *loosely coupled* otherwise. A closely related quantity is the dominance ratio

$$\text{DR} = \frac{k_1}{k_0}, \tag{12}$$

which is smaller than one and can be monotonically mapped onto $\text{E.S.}_1(k)$, thus sharing the same information content (Pázsit and Dykin, 2018).

Concerning the α-eigenvalues, the concept of eigenvalue separation or dominance ratio does not seem to have drawn much attention, to the best of our knowledge, although in the mathematical literature the analogous notion of spectral gap is widely used for eigenvalue problems similar to the α-eigenvalue formulation (for instance in the context of the time-dependent diffusion equation (Bakry and Qian, 2000)). In the same spirit as for the k-eigenvalue problems, we can thus introduce the notion of eigenvalue separation for the α-eigenvalues, which immediately calls for a distinction between 'prompt' and 'delayed' eigenvalues, as mentioned above. In view of these considerations, it seems natural to introduce the *delayed* eigenvalue separation

$$\text{E.S.}_n(\alpha_d) = \text{Re}[\alpha_{d,n}] - \alpha_0, \tag{13}$$

where $\alpha_{d,n}$ is the delayed eigenvalue of order n and α_0 is the fundamental eigenvalue, and the *prompt* eigenvalue separation

$$\text{E.S.}_n(\alpha_p) = \text{Re}[\alpha_{p,n}] - \text{Re}[\alpha_{p,0}], \tag{14}$$

where $\alpha_{p,n}$ is the prompt eigenvalue of order n and $\alpha_{p,0}$ is the prompt eigenvalue with the largest real part.

2.4. Monte Carlo methods

The fundamental mode φ_{k_0} and the fundamental eigenvalue k_0 can be computed by Monte Carlo methods using the standard power iteration method (Goad and Johnston, 1959). The higher-order harmonics of the fission source

$$Q_f(\mathbf{r}) = \int_{4\pi} d\mathbf{\Omega} \int_0^\infty dE\ \bar{\nu}_f(E)\Sigma_f(\mathbf{r}, E)\varphi_k(\mathbf{r}, \mathbf{\Omega}, E), \tag{15}$$

related to the k-eigenvalue problem can be computed by the fission matrix method (Carney et al., 2014). From a physical point of view, the element located at position (m, n) of the $N \times N$ matrix $K_{m,n}$ represents the number of fission neutrons born in region m stemming from one fission neutron born in region n. The fission matrix elements are thus estimated during Monte Carlo simulations by scoring the fission rates in the corresponding spatial cells.

For α-eigenvalue problems in the form of Eq. (10) the fundamental mode φ_{α_0} and the fundamental eigenvalue α_0 can be determined by using a modified α-k power iteration (Zoia et al., 2015). The basic idea is to iteratively search for the dominant α value that makes the α-eigenvalue equation exactly critical with respect to a fictitious k-eigenvalue applied to the production terms. For positive α, a "capture" cross section α/v is taken into account while applying the power iteration (Brockway et al., 1985). For negative α, the contribution $-\alpha/v$ can be interpreted as a "production" term, but this approach is known to suffer from severe numerical instabilities (Hill, 1983). Improved algorithms have been proposed in order to overcome these issues and to take into account the presence of delayed neutrons in the system (Zoia et al., 2014, 2015; Josey, 2018; Mancusi and Zoia, 2018). Recently, matrix-filling Monte Carlo methods have been proposed in order to obtain a discretized version of the α-eigenvalue problem (Betzler et al., 2015, 2018) and improvements have been suggested in order to reduce some bias related to this method (Vitali et al., 2019; Variansyah et al., 2020). Contrary to the fission matrix method, the transport operators of Eq. (5) must be subdivided along space, direction and energy coordinates.

Once the k or α matrices have been filled by Monte Carlo simulation, standard algebra routines are then used in order to obtain the associated eigenvalues and eigenvectors. In this work, we have used the QZ algorithm (Moler and Stewart, 1971). For larger matrix size with high sparsity pattern, iterative algorithms may fail to converge to the correct α spectrum when delayed contributions are included, mainly due to the presence of clusters of eigenvalues.

3. Numerical simulations

In the following, we will explore and compare the properties of E.S.$_n(k)$, E.S.$_n(\alpha_d)$ and E.S.$_n(\alpha_p)$ for a few significant configurations, and will complement this analysis by a careful investigation of the associated fundamental and higher-order eigenmodes. In particular, two families of benchmark configurations have been chosen, respectively homogeneous and heterogeneous, as illustrated in Fig. 2. These systems will be made progressively more decoupled, in the sense previously defined, by acting on the overall system size (for the homogeneous configurations), or on a free parameter. The underlying idea is to ascertain whether the k and α spectral analysis can provide useful information concerning the system response when a parameter related to a decoupling effect is progressively increased. A test-bed Monte Carlo code has been developed in order to estimate the fundamental eigenpairs by standard and $\alpha-k$ power iteration methods and compute the elements of the fission matrix and of the discretized transport operators by the matrix-filling methods described above.

In (Pázsit and Dykin, 2018) it has been pointed out that homogeneous and heterogeneous systems behave differently with respect to eigenvalue separation. For homogeneous systems, small E.S.$_n(k)$ can be attained only by increasing the system size. Under these circumstances, not only E.S.$_1(k)$, but all higher-order E.S.$_n(k)$, $n > 1$, will be small: the physical meaning of this behavior is that many k-eigenmodes will be excited simultaneously. Thus, subject to local perturbations, the system will generally respond with complex space-dependent patterns, where several k-eigenmodes may be present at the same time, and the fundamental eigenmode will not have a privileged role. On the contrary, for heterogeneous systems it is possible to have both a small E.S.$_1(k)$ and much larger higher-order E.S.$_n(k)$, $n > 1$: these configurations are typically obtained in loosely-coupled cores where fissile regions are separated by a sufficiently thick moderator or absorbing layer.

3.1. Geometry and nuclear data definition

The chosen configurations concern multi-group particle transport in 1D geometries, with leakage boundary conditions. The energy domain is partitioned into three groups: fast, epithermal and thermal. Macroscopic cross sections, neutron yields and prompt fission emission spectra have been taken with minimal modifications from the reference (Yamamoto and Sakamoto, 2019), where homogenized materials compatible with real-world fuel assemblies containing UO_2 and water moderator had been proposed. We have then adjusted the velocities and consequently modified the macroscopic cross sections defined for the UO_2 and H_2O materials in order to preserve reaction rates.

Precursor families (which were not available in (Yamamoto and Sakamoto, 2019)) are defined by using the ^{235}U delayed data from the ENDF/B-VI nuclear library (McLane, 2001) recalled in (Cullen, 2004). The average delayed emission energy $\bar{E}_d^j$ is associated to a specific speed $\bar{v}$, which is linearly interpolated between the velocity values (v_1 and v_2, where subscripts indicate the fast and the thermal energy groups, respectively). Emission probabilities for delayed neutrons are linearly interpolated as:

$$\chi_{d1}^j = 1 - \frac{|\bar{v} - v_1|}{v_1 - v_2}, \tag{16}$$

$$\chi_{d2}^j = 1 - \frac{|\bar{v} - v_2|}{v_1 - v_2}, \tag{17}$$

for the first and the second energy group, respectively.

According to these modifications, the properties of the materials UO_2 and H_2O are shown in Tabs. 1, 2 and 3, respectively.

parameters	fast group (g=1)	epithermal group (g=2)	thermal group (g=3)
$v(g)$ [cm/s]	1.66743×10^9	1.73734×10^7	3.46850×10^5
$\Sigma_c(g)$ [cm^{-1}]	3.264×10^{-4}	9.7371×10^{-3}	2.9252×10^{-2}
$\Sigma_f(g)$ [cm^{-1}]	3.0586×10^{-3}	2.1579×10^{-3}	5.6928×10^{-2}
$\Sigma_s(1 \to g)$ [cm^{-1}]	2.21062×10^{-1}	7.3843×10^{-2}	0
$\Sigma_s(2 \to g)$ [cm^{-1}]	0	7.77642×10^{-1}	4.3803×10^{-2}
$\Sigma_s(3 \to g)$ [cm^{-1}]	0	0	1.55272
$\bar{\nu}(g)$ [-]	2.4	2.4	2.4
$\chi_p(g)$ [-]	0.878198	0.121802	0

Table 1: Parameters of the fissile material UO_2 for the heterogeneous configuration.

parameters	1st family	2nd family	3rd family	4th family	5th family	6th family
β_j [pcm]	2.275×10^{1}	1.17455×10^{2}	1.12138×10^{2}	2.51407×10^{2}	1.03077×10^{2}	4.3173×10^{1}
λ_j [cm^{-1}]	1.3336×10^{-2}	3.2739×10^{-2}	1.2078×10^{-1}	3.0278×10^{-1}	8.4949×10^{-1}	2.8530
$\chi_d^j(1)$ [-]	0.52296	0.56487	0.54697	0.61504	0.59265	0.60533
$\chi_d^j(2)$ [-]	0.47704	0.43513	0.45303	0.38496	0.40735	0.39467

Table 2: Delayed neutron parameters of the fissile material UO_2.

parameters	fast group (g=1)	epithermal group (g=2)	thermal group (g=3)
$v(g)$ [cm/s]	1.66743×10^{9}	1.73734×10^{7}	3.46850×10^{5}
$\Sigma_c(g)$ [cm^{-1}]	3.05×10^{-4}	3.699×10^{-4}	1.825×10^{-2}
$\Sigma_s(1 \rightarrow g)$ [cm^{-1}]	2.27125×10^{-1}	1.0464×10^{-1}	0
$\Sigma_s(2 \rightarrow g)$ [cm^{-1}]	0	1.02817	9.7961×10^{-2}
$\Sigma_s(3 \rightarrow g)$ [cm^{-1}]	0	0	2.76295

Table 3: Parameters of the moderator material H_2O for the heterogeneous configuration.

The heterogeneous configurations are composed of two materials, namely UO_2 and H_2O. The homogeneous configurations are characterized by a single representative material obtained by summing the macroscopic cross sections of the fissile and the moderator materials. The properties of this homogenized material are given in Tab. 4.

parameters	fast group (g=1)	epithermal group (g=2)	thermal group (g=3)
$v(g)$ [cm/s]	1.66743×10^{9}	1.73734×10^{7}	3.46850×10^{5}
$\Sigma_c(g)$ [cm^{-1}]	6.314×10^{-4}	1.0107×10^{-2}	4.7502×10^{-2}
$\Sigma_f(g)$ [cm^{-1}]	3.0586×10^{-3}	2.1579×10^{-3}	5.6928×10^{-2}
$\Sigma_s(1 \rightarrow g)$ [cm^{-1}]	4.48187×10^{-1}	1.78483×10^{-1}	0
$\Sigma_s(2 \rightarrow g)$ [cm^{-1}]	0	1.805812	1.41764×10^{-1}
$\Sigma_s(3 \rightarrow g)$ [cm^{-1}]	0	0	1.55272×10^{1}
$\bar{\nu}(g)$ [-]	2.4	2.4	2.4
$\chi_p(g)$ [-]	0.878198	0.121802	4.31567

Table 4: Parameters of the homogenized (UO_2+H_2O) material for the homogeneous configurations.

3.2. Description of the benchmark configurations

The systems will be made progressively more decoupled by acting on the overall system size (for the homogeneous configurations), or on the thickness of the layers (for the heterogeneous configurations). A schematic representation of these configurations is provided in Fig. 2. In order to make our comparisons fair, we have decided to make each configuration critical (i.e., $k_0 = 1$ or equivalently $\alpha_0 = 0$). In practice, this is achieved by adjusting the capture cross section of the fissile material: the computed k_0 must lie close to 1, within 20 pcm uncertainty. Since we set the physical parameters so that the configurations are critical, the fundamental k-eigenmode will coincide with the fundamental α-eigenmode. As a consequence, we can use the regular k power iteration in order to weight the matrix elements required for the α-spectral analysis, which ensures faster convergence of the Monte Carlo methods (Vitali et al., 2019).

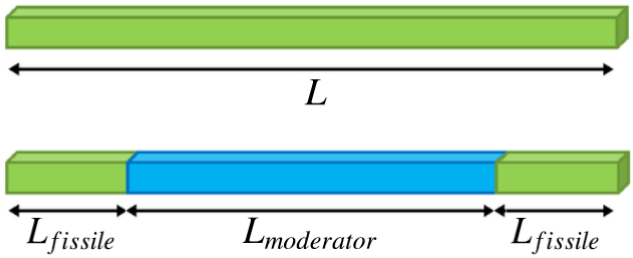

Figure 2: The benchmark configurations for homogeneous (top) and heterogeneous (bottom) 1D systems.

For both the homogeneous and heterogeneous systems, we will investigate 6 different configurations, corresponding to an increasing degree of decoupling. For each case, we will analyze the dominance ratio from Eq. (12), the k-eigenvalue separation from Eq. (11), and the prompt and delayed α-eigenvalue separation using Eqs. (14) and (13).

3.3. Decoupling parameters and critical adjustment

Six cases have been selected for the analysis of homogeneous systems, each defined by a length L ranging from 50 cm to 100 cm. We start our analysis from the largest (the most decoupled) configuration. Then, we adjust the capture cross section, to achieve criticality, by determining the two parameters a and b such that:

$$\Sigma_c' = a\Sigma_c + \frac{b}{v}, \tag{18}$$

for each size of the configuration under analysis. The introduction of the factor b/v allows a finer adjustment with respect to the multiplicative coefficient a. First, b is set to zero in order to compute a such that the system is critical within 100 pcm. Once the factor a is found, the parameter b is set in order to achieve criticality within 20 pcm.

3.3.1. 1D homogeneous configuration

The adjustment to the critical level for the configuration having the largest L has been performed by modifying the macroscopic capture cross section in the fissile material by a parameter a following Eq. (18). Then, we analyzed five additional cases by decreasing the length of the system in order to inhibit the presence of decoupled effects. All cases have been readjusted to the critical level by an iterative search of a coefficient b applied to the macroscopic capture cross section of the fissile material according to Eq. 18.

A value $a = 1.4875$ applied to the macroscopic capture cross section leads to $k_0 = 0.9999 \pm 10^{-4}$ from a k power iteration performed with 2×10^4 particles per cycle and a total of 6×10^3 cycles (5×10^3 active, 10^3 inactive). The values b have been iteratively computed by simulating 5×10^4 particles per cycle and a total of 5×10^3 cycles.

In order to compute the matrix operators in view of the spectral analysis, the length of the domain L has been partitioned into N_x evenly spaced intervals along the x-axis according to Tab. 5. The total size of the matrix ranges from $\sim 6{\times}10^3$ ($L = 50$ cm) to $\sim 1.2{\times}10^4$ ($L = 100$ cm). The fundamental eigenvalues k_0 have been first computed by the k power iteration (see Tab. 6). For these calculations, 10^5 particles per cycle are simulated, for a total of 1.2×10^3 cycles (10^3 active, 2×10^2 inactive). These values allow ensuring the critical state of each configuration, so that the eigenvalue separations will be influenced only by the higher order terms. Then, the eigenvalues computed from the matrix-form of the eigenvalue problem are shown in Tab. 6. All fundamental eigenvalues k_0 computed from the matrix of the corresponding eigenvalue problem are within 2σ standard deviation from the Monte Carlo results obtained from the k power iteration. The k-eigenvalues computed from the k-eigenvalue matrix are used in order to estimate the dominance ratio DR and the eigenvalue separations E.S.$_n(k)$ of the first five orders (Fig. 3). The dominance ratio increases for increasing length of the system from DR = 0.9546 up to DR = 0.9879.

For the α eigenvalue problem, the spatial discretization is again the one given in Tab. 5. The convergence of the α-eigenpairs with respect to the number of spatial intervals has already been analyzed in (Vitali et al., 2019) and will not be discussed here. The cosine of the particle direction with respect to the x-axis has

L [cm]	50	60	70	80	80	100
N_x [-]	500	600	700	800	900	1000

Table 5: Length of the system and number of spatial intervals for the homogeneous configurations.

been uniformly partitioned into $M = 4$ intervals, whereas the energy groups and precursor families have been fixed at $G = 3$ and $J = 6$, respectively. The total size of the matrix for the α-eigenvalue problem ranges from $\sim 9 \times 10^3$ ($L = 50$ cm) to $\sim 2 \times 10^4$ ($L = 100$ cm). The absolute values of the fundamental eigenvalues α_0 are smaller than 2×10^{-3} s^{-1}. For reference, the prompt α eigenvalues computed from the matrix are shown in Tab. 7.

L [cm]	k_0^{MC} [-]	k_0 [-]	k_1 [-]	k_2 [-]	k_3 [-]	k_4 [-]	k_5 [-]
50	$1.0000 \pm 1 \times 10^{-4}$	1.0001	0.9546	0.8856	0.8019	0.7117	0.6221
60	$1.0003 \pm 1 \times 10^{-4}$	1.0002	0.9680	0.9176	0.8539	0.7820	0.7066
70	$1.0002 \pm 1 \times 10^{-4}$	1.0002	0.9760	0.9379	0.8881	0.8304	0.7676
80	$1.0000 \pm 1 \times 10^{-4}$	1.0001	0.9814	0.9514	0.9118	0.8647	0.8123
90	$1.0002 \pm 1 \times 10^{-4}$	1.0002	0.9851	0.9611	0.9289	0.8900	0.8460
100	$0.9999 \pm 1 \times 10^{-4}$	0.9999	0.9878	0.9680	0.9414	0.9090	0.8718

Table 6: First k-eigenvalues for the 1D homogeneous configuration with leakage boundary conditions as a function of the size L of the system. The second column displays the fundamental eigenvalues k_0 computed by Monte Carlo simulation of the power iteration for the k-eigenvalue problem and the corresponding standard deviations. All other eigenvalues have been computed from the matrix-form of the k-eigenvalue problem of the corresponding case.

L [cm]	$\alpha_{p,0}$ [s^{-1}]	$\alpha_{p,1}$ [s^{-1}]	$\alpha_{p,2}$ [s^{-1}]	$\alpha_{p,3}$ [s^{-1}]	$\alpha_{p,4}$ [s^{-1}]	$\alpha_{p,5}$ [s^{-1}]
50	-2.972×10^2	-2.399×10^3	-5.658×10^3	-9.739×10^3	-1.434×10^4	-1.921×10^4
60	-2.926×10^2	-1.783×10^3	-4.157×10^3	-7.217×10^3	-1.078×10^4	-1.466×10^4
70	-2.907×10^2	-1.416×10^3	-3.206×10^3	-5.573×10^3	-8.386×10^3	-1.153×10^4
80	-2.995×10^2	-1.167×10^3	-2.574×10^3	-4.449×10^3	-6.717×10^3	-9.295×10^3
90	-2.949×10^2	-9.951×10^2	-2.119×10^3	-3.640×10^3	-5.499×10^3	-7.638×10^3
100	-3.081×10^2	-8.681×10^2	-1.796×10^3	-3.049×10^3	-4.592×10^3	-6.383×10^3

Table 7: First prompt α-eigenvalues for the 1D homogeneous configuration with leakage boundary conditions as a function of the size L of the system. These values have been computed from the matrix-form of the α-eigenvalue problem of the corresponding case.

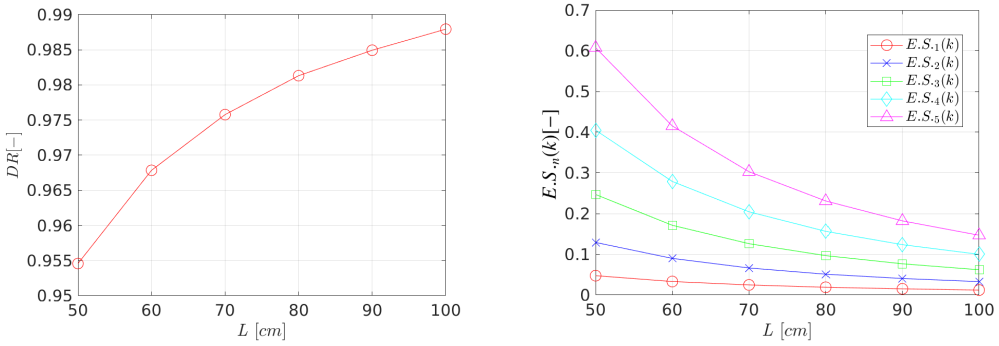

Figure 3: Dominance ratio (left) and k-eigenvalue separations (right) for the 1D homogeneous configuration with leakage boundary conditions as a function of the size L of the system. The first five order of eigenvalue separations are shown, in order, as: E.S.$_1(k)$ red circles, E.S.$_2(k)$ blue crosses, E.S.$_3(k)$ green squares, E.S.$_4(k)$ cyan diamonds and E.S.$_5(k)$ magenta triangles.

The α-eigenvalues computed from the α-eigenvalue matrices are used in order to estimate the delayed E.S.$_n(\alpha_d)$ and the prompt E.S.$_n(\alpha_p)$ eigenvalue separations of the first five orders. The eigenvalue separations E.S.$_n(\alpha_d)$ and the eigenvalue separations E.S.$_n(\alpha_p)$ are shown in Fig. 4.

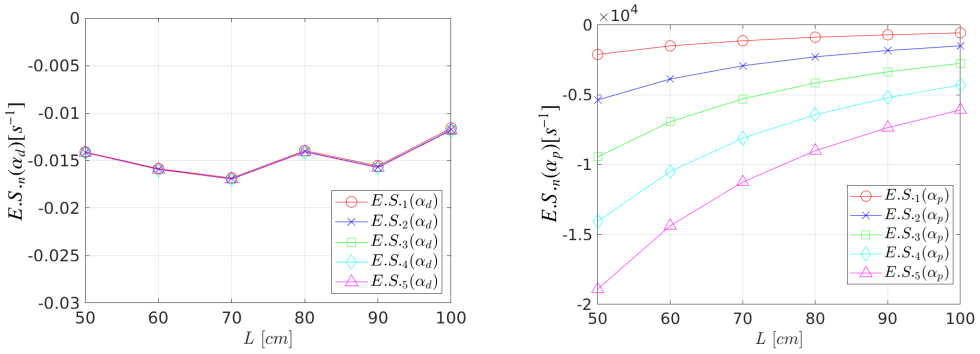

Figure 4: Delayed (left) and prompt (right) α-eigenvalue separations for the 1D homogeneous configuration with leakage boundary conditions as a function of the size L of the system. The first five order of eigenvalue separations are shown, in order, as: E.S.$_1(\alpha)$ red circles, E.S.$_2(\alpha)$ blue crosses, E.S.$_3(\alpha)$ green squares, E.S.$_4(\alpha)$ cyan diamonds and E.S.$_5(\alpha)$ magenta triangles.

The delayed eigenvalue separations (Fig. 4, left) are almost insensitive to the length of the system. This is mainly due to the presence of the clusters of the delayed eigenvalues. Conversely, and quite surprisingly, the behaviour of the prompt α-eigenvalue separations (Fig. 4, right) is qualitatively similar to the k-eigenvalue separations.

The spatial profiles of the corresponding eigenmodes are not shown here, since they turn out to be weakly dependent on the eigenvalue formulation and on the length of the system. The delayed α-eigenmodes of the dominant order display a spatial distribution close to that of the corresponding prompt α-eigenmodes, as expected from (Sanchez and Tomatis, 2019). Moreover, the eigenmodes related to the precursor concentrations of the fundamental order are positive, whereas those associated to the dominant eigenvalue of each delayed cluster change sign.

3.3.2. 1D heterogeneous configuration

The occurrence of decoupling effects for heterogeneous configurations can be observed when neutrons are localized into distinct regions (Pázsit and Dykin, 2018). A perturbation induced in a specific location of the system has to overcome such spatial barriers in order to reach the other regions. We consider here a three-region slab geometry where two fissile regions (of length $L_{\text{fissile}} = 20$ cm, respectively) are separated by a progressively larger moderator region (of length $L_{\text{moderator}}$). Six cases have been selected for our analysis, with the total length of the geometry $L = 2L_{\text{fissile}} + L_{\text{moderator}}$. The choice of this configuration was inspired by the three-region slab geometry benchmark problem analyzed in (Yamamoto and Nomura, 2001). The material properties describing these regions have been shown in Tabs. 1 and 2 for the fissile material and in Tab. 3 for the moderator material.

The first step of our analysis consists in the search of a critical configuration by k power iteration. The adjustment to the critical level is performed by modifying the macroscopic capture cross section in the fissile material following Eq. (18), as previously detailed for the homogeneous configuration. We analyzed five cases by decreasing the length of the moderator region in order to increase the coupling between the fissile regions.

We start by considering a configuration characterized by regions having equal width. The emergence of decoupling effect was observed for a 20 cm long slab region in (Yamamoto and Nomura, 2001), hence the length of the system will be set to 60 cm. A value $a = 1.167$ applied to the macroscopic capture cross section of the fissile regions leads to $k_0 = 1.0002 \pm 4 \times 10^{-4}$ from a k power iteration performed with 2×10^4 particles per cycle and a total of 6×10^2 cycles (5×10^2 active, 10^2 inactive). Five smaller lengths of the moderator region have been also considered: 15 cm, 10 cm, 7 cm, 5 cm and 2 cm, respectively. The coefficient b from Eq. (18) has been iteratively computed by simulating 5×10^4 particles per cycle and a total of 2×10^3 cycles.

In order to compute the matrix operators for the spectral analysis, the length

of the domain L has been partitioned into N_x evenly spaced intervals along the x-axis according to Tab. 8. The size of the matrix correspondingly ranges from $\sim 1 \times 10^4$ ($L = 40$ cm) to $\sim 1.4 \times 10^4$ ($L = 60$ cm). The fundamental eigenvalues k_0 have been first computed by the k power iteration (see Tab. 9). For these calculations, 10^5 particles per cycle are simulated, for a total of 1.2×10^3 cycles (10^3 active, 2×10^2 inactive). Similarly as for the homogeneous case, these values have been computed in order to calibrate each configuration at the critical state, so that all eigenvalue separations will be influenced only by the higher order eigenvalues. The eigenvalues computed from the matrix-form of the eigenvalue problem are shown in Tab. 9. All fundamental eigenvalues k_0 computed from the matrix are within 2σ standard deviation from the Monte Carlo results obtained from the k power iteration. The k-eigenvalues computed from the k-eigenvalue matrix are used in order to estimate the dominance ratio DR and the eigenvalue separations E.S.$_n(k)$ of the first five orders (Fig. 5). The values of the dominance ratio increase for increasing length of the moderator from DR = 0.7908 up to DR = 0.9971. The eigenvalue separation E.S.$_1(k)$ for this heterogeneous configuration decreases for increasing length of the moderator. Contrary to the results observed for the homogeneous configurations, the higher-order eigenvalue separations E.S.$_n(k)$, $n > 1$, are much larger than the first-order E.S.$(k)_1$; moreover, E.S.$_{2n+1}(k)$ converges to E.S.$_{2n}(k)$ for stronger decoupling between the fissile regions (Fig. 5). This convergence pattern is induced by the symmetry of the system, the two fissile region being of equal length.

L [cm]	40	45	50	55	60
N_x [-]	800	900	1000	1100	1200

Table 8: Length of the system and number of spatial intervals for the heterogeneous configurations.

For α eigenvalue problems, N_x are again taken from Tab. 8. The cosine of the particle direction with respect to the x-axis has been uniformly partitioned into $M_x = 4$ intervals, whereas the energy groups and precursor families have been fixed at $G = 3$ and $J = 6$, respectively. The total size of the matrix for the α-eigenvalue problem ranges from $\sim 1.5 \times 10^4$ ($L = 40$ cm) to $\sim 2 \times 10^4$ ($L = 60$ cm). The absolute values of the fundamental eigenvalues α_0 are smaller than 2.5×10^{-3} s^{-1}. For reference, the prompt eigenvalues computed from the matrix-form of the eigenvalue problem are shown in Tab. 10.

The α-eigenvalues computed from the α-eigenvalue matrix problem are used in order to estimate the delayed E.S.$_n(\alpha_d)$ and the prompt E.S.$_n(\alpha_p)$ eigenvalue separations of the first five orders. The delayed eigenvalue separations (Fig. 6,

L [cm]	k_0^{MC} [-]	k_0 [-]	k_1 [-]	k_2 [-]	k_3 [-]	k_4 [-]	k_5 [-]
42	$0.9997 \pm 2 \times 10^{-4}$	0.9999	0.7907	0.5538	0.3909	0.2600	0.1904
45	$1.0003 \pm 2 \times 10^{-4}$	1.0001	0.8669	0.5699	0.4539	0.2726	0.2252
47	$1.0000 \pm 2 \times 10^{-4}$	1.0001	0.9122	0.5700	0.4891	0.2750	0.2422
50	$1.0002 \pm 2 \times 10^{-4}$	1.0001	0.9571	0.5650	0.5234	0.2747	0.2577
55	$0.9996 \pm 2 \times 10^{-4}$	0.9998	0.9882	0.5585	0.5469	0.2725	0.2676
60	$0.9999 \pm 2 \times 10^{-4}$	0.9998	0.9969	0.5563	0.5533	0.2716	0.2703

Table 9: First k-eigenvalues for the 1D heterogeneous configuration as a function of the size L of the system. The second column displays the fundamental eigenvalues k_0 computed by Monte Carlo simulation of the power iteration for the k-eigenvalue problem and the corresponding standard deviations. All other eigenvalues have been computed from the matrix-form of linear transport operator corresponding to the k-eigenvalue problem.

L [cm]	$\alpha_{p,0}$ [s^{-1}]	$\alpha_{p,1}$ [s^{-1}]	$\alpha_{p,2}$ [s^{-1}]	$\alpha_{p,3}$ [s^{-1}]	$\alpha_{p,4}$ [s^{-1}]	$\alpha_{p,5}$ [s^{-1}]
42	-2.419×10^2	-9.153×10^3	-1.716×10^4	-2.791×10^4	-3.332×10^4	-4.229×10^4
45	-1.900×10^2	-5.471×10^3	-1.211×10^4	-2.164×10^4	-2.708×10^4	-3.382×10^4
47	-1.874×10^2	-3.470×10^3	-1.025×10^4	-1.757×10^4	-2.403×10^4	-2.927×10^4
50	-1.908×10^2	-1.686×10^3	-8.744×10^3	-1.359×10^4	-2.017×10^4	-2.509×10^4
55	-2.076×10^2	-5.880×10^2	-7.671×10^3	-1.051×10^4	-1.514×10^4	-2.035×10^4
60	-2.115×10^2	-3.062×10^2	-7.196×10^3	-9.122×10^3	-1.218×10^4	-1.635×10^4

Table 10: First prompt α-eigenvalues for the 1D heterogeneous configuration as a function of the size L of the system. These values have been computed from the matrix-form of linear transport operator corresponding to the α-eigenvalue problem.

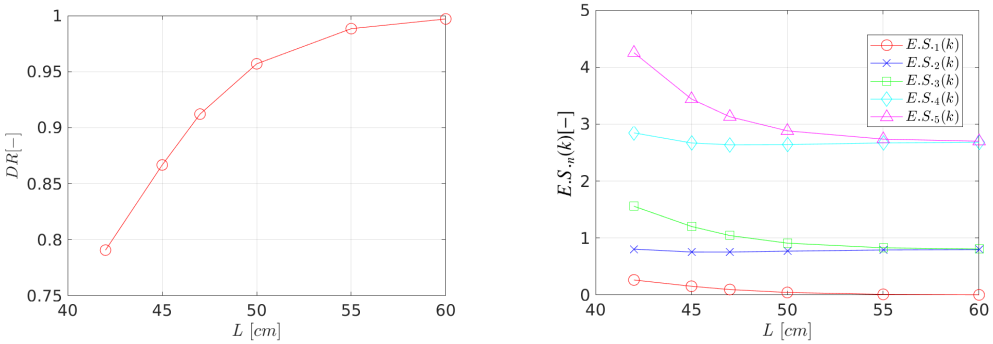

Figure 5: Dominance ratio (left) and k-eigenvalue separations (right) for the 1D heterogeneous configuration as a function of the size L of the system. The first five order of eigenvalue separations are shown, in order, as: E.S.$_1(k)$ red circles, E.S.$_2(k)$ blue crosses, E.S.$_3(k)$ green squares, E.S.$_4(k)$ cyan diamonds and E.S.$_5(k)$ magenta triangles.

left) are again almost insensitive to the length of the moderator. The prompt α-eigenvalue separations (Fig. 6, right) have a distinct behaviour as opposed to the k-eigenvalue separations. Moreover, also E.S.$(\alpha_p)_{2n+1}$ will probably converge to E.S.$(\alpha_p)_{2n}$, but a larger gap is observed between these two orders of eigenvalue separations with respect to the k-eigenvalue separations of the corresponding orders. These results are inherently due to the presence of a non-fissile region for this heterogeneous configuration. Thermal neutrons diffusing in the moderator region, or fast neutrons crossing the moderator region, have a different time scale with respect to those travelling through the fissile regions. Such differences have an impact on the α-eigenvalues, which are sensitive to the time scales of the system, contrary to k-eigenvalues.

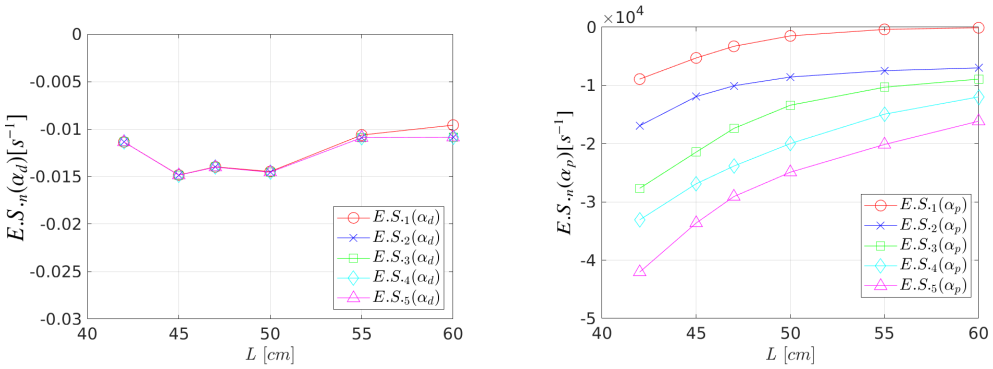

Figure 6: Delayed (left) and prompt (right) α-eigenvalue separations for the 1D heterogeneous configuration as a function of the size L of the system. The first five order of eigenvalue separations are shown, in order, as: E.S.$_1$ red circles, E.S.$_2$ blue crosses, E.S.$_3$ green squares, E.S.$_4$ cyan diamonds and E.S.$_5$ magenta triangles.

The corresponding fundamental (Fig. 7) and first-order (Fig. 8) eigenmodes are examined for k and α eigenvalue formulations. By inspection of the fundamental eigenfunction, the central region of the system over-moderates for small length of the moderator region (from $L = 42$ cm, up to $L = 47$ cm). For larger sizes of the central region, the over-moderation effects are progressively less apparent, and are mainly located at the boundaries with the fissile material. The spatial shape drops in the central region, decoupling the system behaviour into two distinct spatial regions (from $L = 50$ cm, up to $L = 60$ cm). The eigenmodes are weakly sensitive to the eigenvalue formulation and to the length of the system. Similarly to the results obtained from the 1D homogeneous configuration, the delayed α-eigenmodes of the dominant order display a spatial distribution close to that of the corresponding prompt α-eigenmodes. Furthermore, the eigenmodes related to the precursor concentrations of the fundamental

order are positive, whereas those associated to the dominant eigenvalue of each delayed cluster change sign.

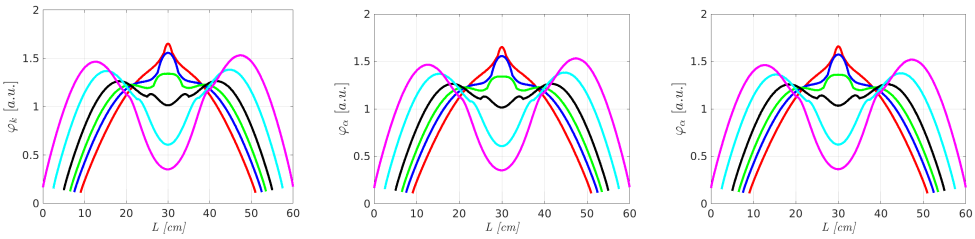

Figure 7: Spatial distribution of the k (left), α (center) and prompt α (right) fundamental eigenmodes for the 1D heterogeneous as a function of the size L of the system. Color legend according to the ascending order of the size L of the system is: $L = 42$ cm red, $L = 45$ cm blue, $L = 47$ cm green, $L = 50$ cm black, $L = 55$ cm cyan and $L = 60$ cm magenta.

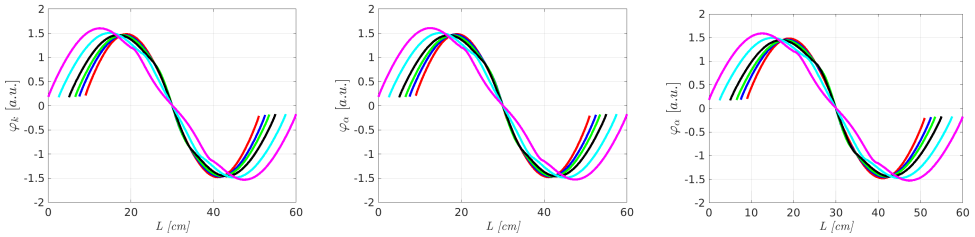

Figure 8: Spatial distribution of the k (left), α (center) and prompt α first-order eigenmodes for the 1D heterogeneous as a function of the size L of the system. Color legend according to the ascending order of the size L of the system is: $L = 42$ cm red, $L = 45$ cm blue, $L = 47$ cm green, $L = 50$ cm black, $L = 55$ cm cyan and $L = 60$ cm magenta.

4. An application to the EOLE critical facility

We have developed the aforementioned matrix-filling methods in TRIPOLI-4®, in view of carrying out spectral analysis in continuous-energy Monte Carlo transport with complex geometries. In this respect, we have chosen to revisit the EPILOGUE experimental campaign, which was the last one to be performed in the EOLE critical facility at CEA Cadarache. The EPILOGUE campaign was especially conceived in order to ascertain whether heterogeneities and decoupling effects might occur in small reactor cores, with the aim of preparing the investigation of similar effects in large cores of Generation III+ reactors. Among the configurations analyzed during this campaign, the 'water blade' setup (shown in Figure 9) was prepared by replacing a row and a column of fuel pins by moderator (the 'blade').

4.1. Experimental and numerical configurations

The main aim of the water blade is to achieve a local over-moderation effect in the core region. In principle, the water layer substituting a section of fuel pins should separate the radial neutron flux into two distinct regions. We will thus probe by the matrix-filling methods how the presence of the water blade affects the spectrum of the Boltzmann equation. Moreover, we will numerically explore by Monte Carlo simulation the effects of adding two additional water blades (obtained by replacing more fuel pins with light borated water), with the aim of enhancing the decoupling of the core region.

Figure 9 shows the radial section of the two new setups that will be called for shortness '2 water blades' configuration (left) and '3 water blades' configuration (right). In the following, by analogy we will define the (single) water blade configuration as the '1 water blade' configuration. As a reference, we will also consider the configuration without water blades.

All these EPILOGUE cores have been simulated by using TRIPOLI-4®. Before detailing the simulation parameters of such calculations, a preliminary step is required in order to make the systems critical (similarly as done in Sec. 3). In order to achieve this condition, we modified the Boron concentration in the moderator of each configuration. This procedure can be performed in TRIPOLI-4® by a critical Boron concentration search routine, which iteratively seeks a multiplier coefficient for the Boron concentration C_{Boron}. For these calculations, 10^5 particles are simulated, for a total of 1.5×10^3 cycles (10^3 active, 5×10^2 discarded). Water composition and Boron concentration of the moderator for each configuration are shown in Tab. 11.

water blades [-]	0	1	2	3
H_1 [atoms/(barn × cm)]	4.675×10^{-5}	3.923×10^{-5}	3.923×10^{-5}	3.923×10^{-5}
H_{1,H_2O} [atoms/(barn × cm)]	6.669×10^{-2}	6.670×10^{-2}	6.670×10^{-2}	6.670×10^{-2}
O_{16} [atoms/(barn × cm)]	3.339×10^{-2}	3.339×10^{-2}	3.339×10^{-2}	3.339×10^{-2}
B_{10} [atoms/(barn × cm)]	3.286×10^{-6}	2.708×10^{-6}	1.878×10^{-6}	7.339×10^{-7}
B_{11} [atoms/(barn × cm)]	1.323×10^{-5}	1.090×10^{-5}	7.561×10^{-6}	2.954×10^{-6}
C_{Boron} [ppm]	296.7	244.5	169.6	66.3

Table 11: Water composition and Boron concentration (ppm) of the moderator in water blade configurations.

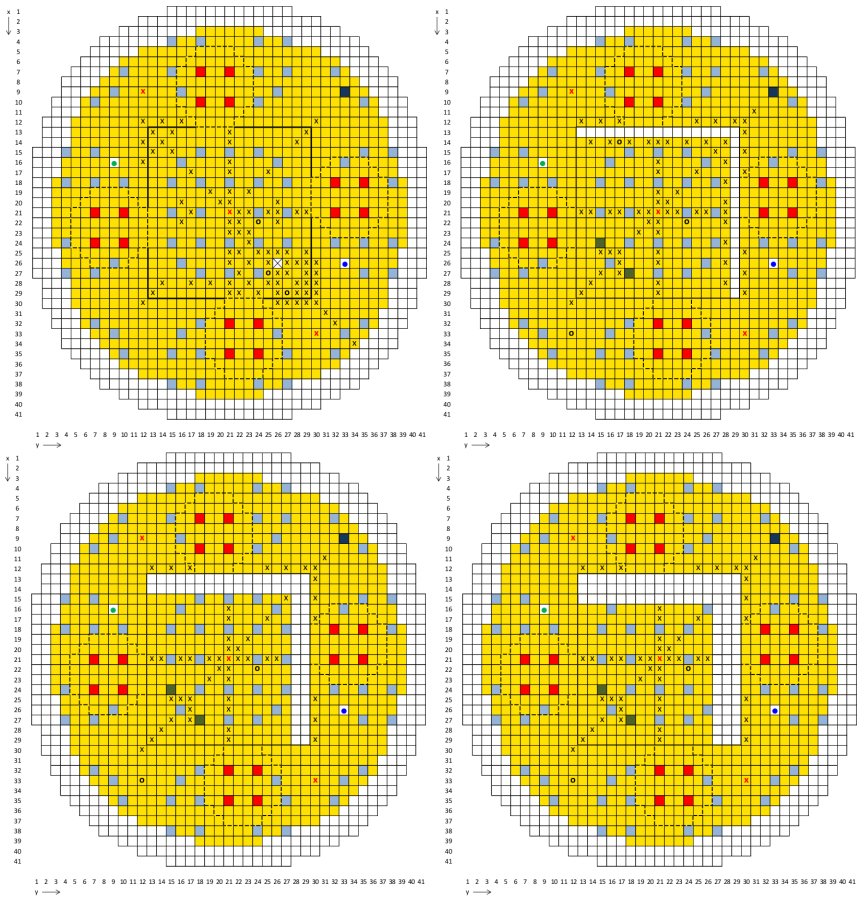

Figure 9: Schematic radial section of the EOLE reactor in water blade configurations. The ‘1 water blade’ configuration (top-right) is arranged by removing two lines of fuel pins and by inserting B_4C rods (olive green) in the ‘reference’ configuration (top-left). The ‘2 water blades’ configuration (bottom-left) and the ‘3 water blades’ configuration (bottom-right) are arranged by removing four and six lines of fuel pins from the core region. Fuel elements of enriched UO_2 at 3.7% are colored in yellow and are distinguished in monitored fuel elements (black cross, black circle and red cross). Locations for control rods (red), pilot rod (dark blue) and B_4C rods (olive green) are shown. Two fission chambers are shown: CF2268 (white, green circle) and CF2269 (white, blue circle). All the remaining elements are filled with borated light water (light grey).

The discretization of the phase-space variables for the EPILOGUE configurations implies large matrix sizes for the eigenvalue formulations. In order to detect the effect of the moderator heterogeneity, we have chosen to primarily use a finer mesh for the spatial coordinates in the radial section of the reactor. The effect of the water blade is indeed expected to be more apparent on the radial plane than on the axial coordinate. By fixing the origin of the spatial reference system in the center of the reactor, a uniform Cartesian grid is applied on the radial plane, dividing the two coordinates in $N_x = N_y = 48$ spatial bins from -52.8 cm to 52.8 cm. The axial coordinate is integrated over the whole height of the system ($N_z = 1$). The angle discretization is kept at $M_x = M_y = 2$ and $M_z = 1$. The energy domain is divided into $G = 3$ groups: a fast region in the interval [20 MeV, 94.66 keV], an epithermal region [94.66 keV, 0.625 eV] and a thermal region [0.625 eV, 10^{-5} eV]. Nuclear data are taken from the JEFF 3.1.1 library (Santamarina et al., 2009), with the same $J = 8$ precursors families for all fissile nuclei. The total number of elements of the matrix for the α-eigenvalue problem is about 2×10^9.

As for the k-eigenvalue problem, we used the fission matrix capability of Tripoli-4®. The eigenmodes computed from the fission matrix represent fission rates (thus non-vanishing only in the fissile regions of the core), which implies a significant reduction of the matrix size. In particular, we impose a Cartesian grid on the radial section of the core region, specifically $N_x = N_y = 74$ from -23.31 cm to 23.31 cm along both axes. Then, the spatial bins perfectly overlap on the square fuel pins section (1.26×1.26 cm^2). The total number of elements of the fission matrix is about 3×10^7.

4.2. Eigenvalue analysis

The Boron concentrations shown in Tab. 11 are used in order to achieve criticality. All the results presented in the following have been obtained during a standard power iteration that was used to estimate the elements of the matrices needed for the α- and k- spectral analysis. In particular, 10^5 particles per cycle were simulated for a total of 2.5×10^3 cycles (2×10^3 active, 5×10^2 discarded).

The fundamental eigenvalues obtained with these calculations were less than 20 pcm from criticality, with a standard deviation of 7 pcm. These values have been computed in order to assess the critical state of all the configurations. This allows analyzing the eigenvalue separations of each configuration by fixing the fundamental order. During the same calculations, the discretized operators have been estimated and post-processed in order to obtain the matrices of the α-eigenvalue problems. The real parts of the corresponding eigenvalues have been

arranged in descending order in order to discriminate the fundamental eigenvalue, the delayed eigenvalues and the prompt eigenvalues. The delayed eigenvalues cluster close to (minus) the decay constants equal to $\min(\lambda) = 1.247\times10^{-2}$ s^{-1}. Conversely, the first five prompt α-eigenvalues exhibit significant variations as a function of the configuration and of the mode order. The eigenvalues computed for these configurations were combined in order to obtain the dominance ratio and the eigenvalue separation according to the k- and the α-formulations. These values are shown in Figs. 10 and 11.

The dominance ratio slightly increases for a larger thickness of the water blade from DR = 0.7080 up to DR = 0.7449 which suggests the absence of strong decoupling effects in all these configurations. We observe that for these 2D configurations the first and second, fourth and fifth orders of eigenvalue separations of the k-formulation are extremely close. This feature is related to the symmetry of the core, which in turn induces a degeneracy in the eigenvalues. Conversely, the eigenvalue separations do not change significantly with respect to the number of water blades.

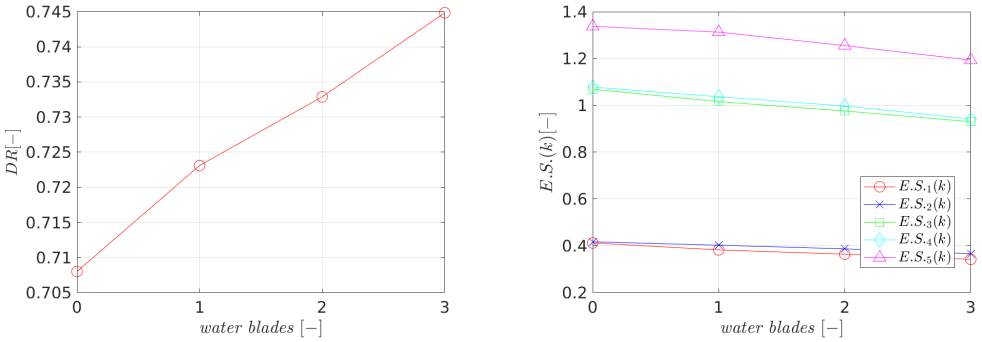

Figure 10: Dominance ratio (left) and k-eigenvalue separations (right) for EOLE water blade configurations. The first five order of eigenvalue separations are shown, in order, as: E.S.$_1(k)$ red circles, E.S.$_2(k)$ blue crosses, E.S.$_3(k)$ green squares, E.S.$_4(k)$ cyan diamonds and E.S.$_5(k)$ magenta triangles.

The delayed E.S.$_n(\alpha_d)$ and the prompt E.S.$_n(\alpha_p)$ eigenvalue separations of the first five orders are displayed in Fig. 11. The delayed eigenvalue separations are almost constant as a function of the number of water blades. The prompt α-eigenvalue separations have a different behaviour than the k-eigenvalue separations. In particular, the eigenvalue separations associated to the '0 water blade' configuration appear to have a different trend with respect to the results obtained for the configurations with blades. This stems from the reference configuration not having any noticeable heterogeneity along the spatial coordinates. For

the configurations containing the water blades, on the contrary, we notice a behaviour similar to the one for the k-eigenvalue separations. The proximity of the first and second, third and fourth order of the eigenvalue separations suggests again a degeneracy effect related to the symmetry of the core.

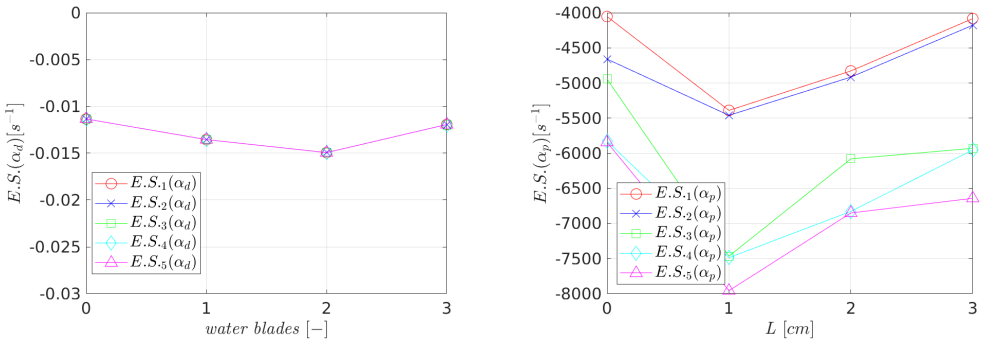

Figure 11: Delayed (left) and prompt (right) α-eigenvalue separations for EOLE water blade configurations. The first five order of eigenvalue separations are shown, in order, as: E.S.$_1(\alpha)$ red circles, E.S.$_2(\alpha)$ blue crosses, E.S.$_3(\alpha)$ green squares, E.S.$_4(\alpha)$ cyan diamonds and E.S.$_5(\alpha)$ magenta triangles.

4.3. Eigenmode analysis

We will now examine the eigenvectors corresponding to the k- and the α-eigenvalue formulation as a function of the spatial coordinates in the cross-section plane of the EPILOGUE cores. A finer discretization is applied in the fissile regions, since fission rates $Q_{f,k}(x,y)$ depend only on the spatial coordinates. Conversely, α-eigenfunctions are related to particle population (neutrons and precursors), thus requiring the discretization of the whole phase-space, yielding distributions of the kind $\varphi_\alpha(x,y,\mu_x,\mu_y,E)$ for neutrons and $c_{j,\alpha}(x,y,E)$ for precursors.

Figure 12 shows the fundamental eigenmodes according to both α- and k-eigenvalue formulations for each configuration. The influence of both the water blade and of the B_4C control rods increases with increasing number of blades. In particular, the fundamental eigenmode φ_{α_0} is larger in the water blade layer, and is depressed in the control rods regions. The fission rates Q_{f,k_0} are larger in the proximity of the water blade region, proving the over-moderation effect caused by the moderator.

The first-order eigenfunctions are shown in Figure 13: the presence of a node smoothens the distortions caused by the heterogeneity. In particular, the distortion caused by the spatial heterogeneity of the system disappears when consid-

ering the α-eigenmodes, whereas its effect is immediately apparent in the fission rates obtained according to the k-eigenvalue formulation. The thermal and the fast energy ranges have been considered in order to enhance the effect caused by the spatial heterogeneity of the system on the fundamental eigenmode φ_{α_0} shown in Fig. 14. The distribution for the '0 water blade configuration' in the thermal energy range is larger on the peripheral zone just outside the core and in its center. The fast component of the eigenmodes displays a Bessel-like shape. In the thermal energy range, the flux distribution located inside the water blade region becomes larger for increasing thickness of the water layer. This effect can be justified by the stronger over-moderation induced by the gradually larger number of replaced fuel pins. In the fast region, the moderator acts as an absorber and a decrease of the neutron flux is observed by increasing the number of blades.

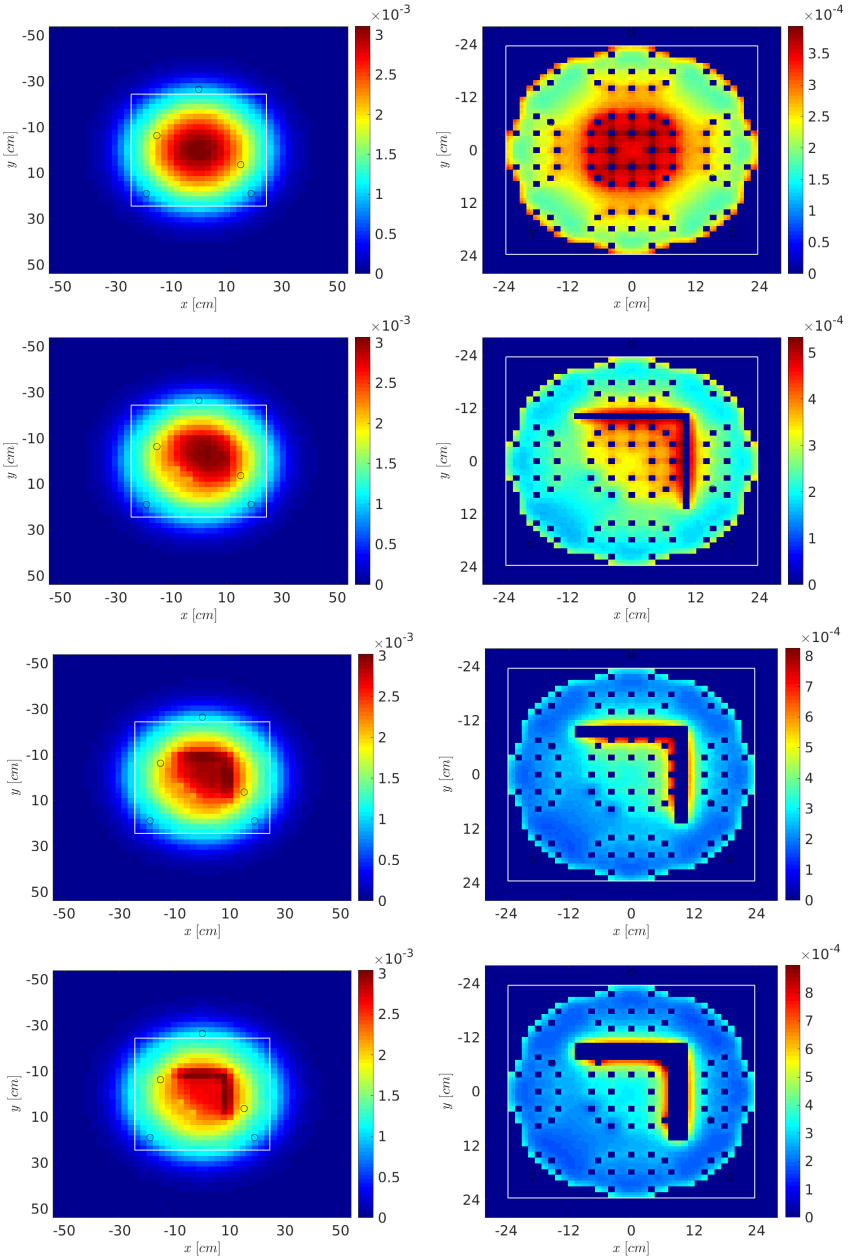

Figure 12: Spatial behaviour of the forward fundamental eigenmodes $\varphi_{\alpha_0}(x, y, g)$ (left column) and $Q_{f,k_0}(x, y)$ (right column) on the EOLE cross section. From top to bottom, configurations with 0 (first row), 1 (second row), 2 (third row) and 3 (fourth row) water blades are shown. The spatial eigenfunctions have been integrated in the whole energy region. All the eigenfunctions have been normalized. Detector positions of the water blade configuration are shown as black circles. To guide the eye, the portion of the core within the white frame is the same.

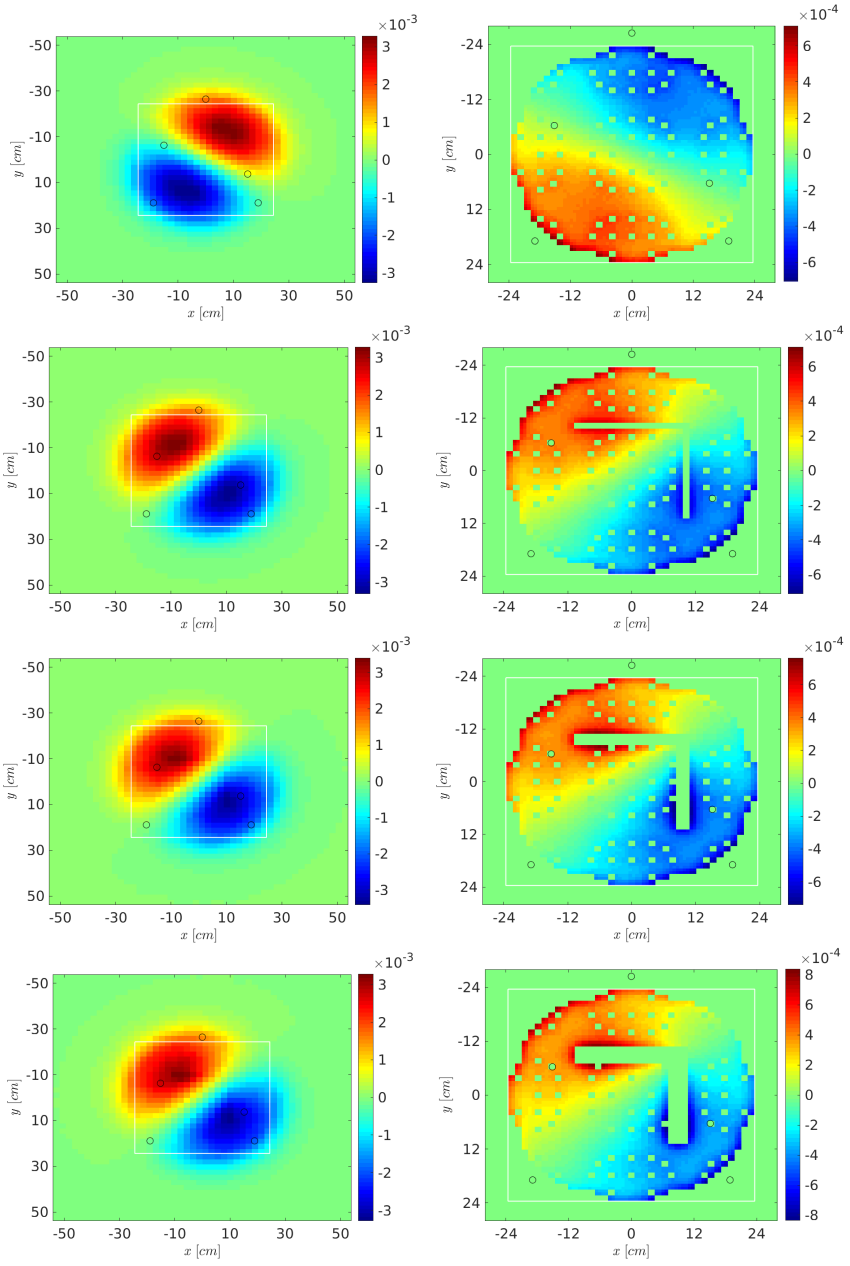

Figure 13: Spatial behaviour of the forward first order eigenmodes $\varphi_{\alpha_1}(x, y, g)$ (left column) and $Q_{f,k_1}(x, y)$ (right column) on the EOLE cross section. From top to bottom, configurations with 0 (first row), 1 (second row), 2 (third row) and 3 (fourth row) water blades are shown. The spatial eigenfunctions have been integrated in the whole energy region. All the eigenfunctions have been normalized. Detector positions of the water blade configuration are shown as black circles. To guide the eye, the portion of the core within the white frame is the same.

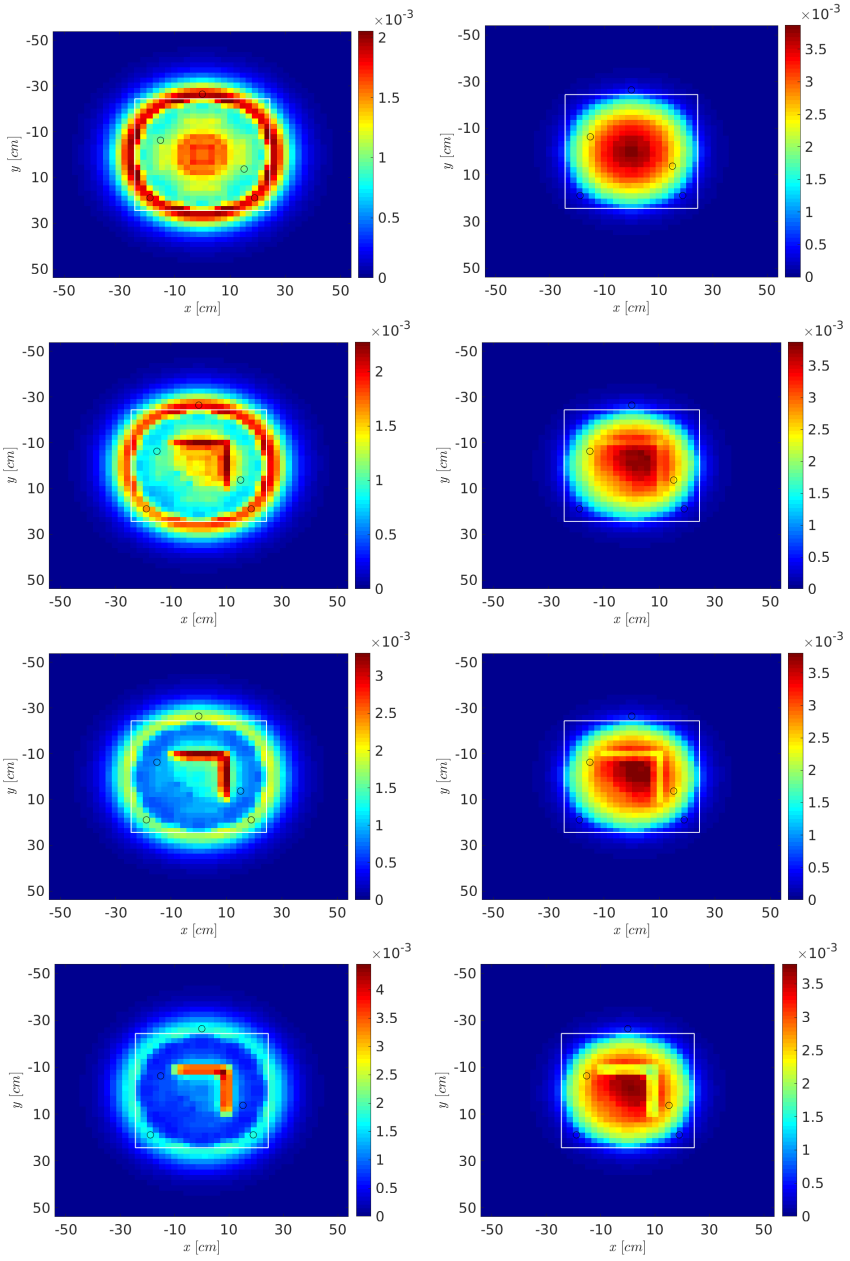

Figure 14: Spatial behaviour of the forward fundamental eigenmodes $\varphi_{\alpha_0}(x, y, g)$ integrated over the thermal (left column) and the fast (right column) energy ranges on the EOLE cross section. From top to bottom, configurations with 0 (first row), 1 (second row), 2 (third row) and 3 (fourth row) water blades are shown. All the eigenfunctions have been normalized. Detector positions of the water blade configuration are shown as black circles. To guide the eye, the portion of the core within the white frame is the same.

5. Conclusions

Eigenvalue separation can conveniently convey information on the degree of decoupling of a reactor core. In this paper, we showed that spectral analysis performed by matrix-filling Monte Carlo methods provides a useful tool for the investigation of decoupling effects. For this purpose, we have selected a few benchmark configurations covering homogeneous and heterogeneous systems. Consistently with k-eigenvalue separations (Pázsit and Dykin, 2018), our Monte Carlo simulations have shown that homogeneous and heterogeneous systems behave differently with respect to the decoupling parameter, in particular concerning higher-order eigenvalue separations. The delayed α-eigenvalues are rather insensitive to the decoupling parameter, and can hardly be used as a reliable estimator to detect such effects. On the contrary, prompt α-eigenvalues respond to the decoupling parameter in a way that is qualitatively similar to the k-eigenvalue for the homogeneous configurations, and might be thus usefully adopted as a complement to the classical k-eigenvalue separations for core design. A distinct behaviour was found for the prompt α-eigenvalue separation and the k-eigenvalue separation for the heterogeneous configurations.

In order to highlight the role of the spectral analysis in the characterization of real-world nuclear systems, we investigated spatial decoupling effects by means of Monte Carlo simulation for the EPILOGUE program in the EOLE critical facility. We focused in particular on the so-called 'water blade' configuration, where a local heterogeneity was introduced in the core, in view of exacerbating decoupling effects during rod drop experiments. Moreover, we complemented our simulations of the 'single blade' configuration by adding further water blades.

The over-moderation caused by the presence of the water layer does have an impact on the k- and α-eigenvalues. Despite relatively small variations from the reference configuration, the dominance ratio and the eigenvalue separation suggest the presence of a weak decoupling effect. This statement is also supported by the analysis of the spatial shape of both k- and α-eigenmodes. Experimental measurements did not provide qualitative results related to the influence of such effect. For this reason, in our Monte Carlo simulations the layer of the water blade region has been increased by considering additional configurations in order to enhance the decoupling between the two fissile areas. Overall, the effects induced by the heterogeneity of the system are clearly detected by the spectral analysis. Nonetheless, our numerical findings seem to point out that the decoupling effects are rather mild and do not separate the system into two loosely-coupled cores, even in the rather extreme case of 3 water blades.

Although the EOLE facility is now definitively shut down, the know-how stemming from the spectral analysis methodology will be key for any dedicated future experimental programs in Zero-Power Reactors (ZPR). This approach can be applied among others to the analysis of space-time dynamic responses for both critical and sub-critical (i.e., fuel loading or ADS) systems, detector optimization in large Gen-III cores, or the criticality analysis of loosely coupled systems such as spent fuel pools and reprocessing sites. The comparisons between higher-order eigenpairs according to α and k formulations will be further explored in future work in the context of the CROCUS and SPERT III benchmarks (Zoia et al., 2016; Nauchi et al., 2020; Zoia and Brun, 2016).

Acknowledgements

TRIPOLI-4 ® is a registered trademark of CEA. A. Jinaphanh and A. Zoia wish to thank EDF for partial financial support.

References

Y. Asahi. Theory of Omega-d, Modes. *Journal of Science and Technology*, 12:92–106, 1975.

D. Bakry and Z. Qian. Some New Results on Eigenvectors via Dimension, Diameter, and Ricci Curvature. *Advances in Mathematics*, 155:98–153, 2000.

W. D. Beckner and R. A. Rydin. Higher-order relationship between static power tilts and eigenvalue separation in nuclear-reactors. *Nuclear Science and Engineering*, 56:131–141, 1975.

G. Bell and S. Glasstone. *Nuclear Reactor Theory*. Van Nordstrand Reinhold Company, 1970.

B. R. Betzler, W. R. Martin, B. C. Kiedrowski, and F. B. Brown. Calculating Alpha Eigenvalues of One-Dimensional Media with Monte Carlo. *Journal of Computational and Theoretical Transport*, 43:38–49, 2014.

B. R. Betzler, B. C. Kiedrowski, F. B. Brown, and W. R. Martin. Calculating Infinite-medium Alpha-eigenvalue Spectra with Monte Carlo using a Transition Rate Matrix Method. *Nuclear Engineering and Design*, 295:639–644, 2015.

B. R. Betzler, B. C. Kiedrowski, W. R. Martin, and F. B. Brown. Calculating Alpha Eigenvalues and Eigenfunctions with a Markov Transition Rate Matrix Monte Carlo Method. *Nuclear Science and Engineering*, 192:115–152, 2018.

D. Brockway, P. Soran, and P. Whalen. Monte Carlo alpha calculations. Technical Report LA-UR-85-1224, Los Alamos National Laboratory, 1985.

S. Carney, F. Brown, B. Kiedrowski, and W. Martin. Theory and applications of the fission matrix method for continuous-energy Monte Carlo. *Annals of Nuclear Energy*, 73:423–431, 2014.

N. Corngold. Some Transient Phenomena in Thermalization I. Theory. *Nuclear Science and Engineering*, 19:80–90, 1964.

D. E. Cullen. A Simple Model of Delayed Neutron Emission. Technical Report UCRL-TR-204743, University of California, Lawrence Livermore National Laboratory, 2004.

J. J. Duderstadt and W. R. Martin. *Transport theory*. J. Wiley and sons, New York, 1979.

D. D. Ebert, J. Clemence, and W. M. S. Jr. Interpretation of coherence function measurements in zero-power coupled-core reactors. *Nuclear Science and Engineering*, 55:380–386, 1974.

F. Filiciotto, A. Jinaphanh, and A. Zoia. Super-history methods for adjoint-weighted tallies in monte carlo time eigenvalue calculations. In *Proceedings of PHYSOR 2020*, 2020.

L. R. Foulke and E. P. Gyftopoulos. Application of the Natural Mode Approximation to Space-Time Reactor Problems. *Nuclear Science and Engineering*, 30:419–435, 1967.

W. Goad and R. Johnston. A Monte Carlo Method for Criticality Problems. *Nuclear Science and Engineering*, 5:371–375, 1959.

K. Hashimoto, T. Ohsawa, R. Miki, and T. Shibata. A practical formula for inferring eigenvalue separation from flux tilt measurements in nuclear-reactors. *Annals of Nuclear Energy*, 18(3): 131–140, 1991.

A. F. Henry. The Application of Inhour Modes to the Description of Non-Separable Reactor Transients. *Nuclear Science and Engineering*, 20:338–351, 1964.

T. R. Hill. Efficient methods for time absorption (alpha) eigenvalue calculations. Technical Report LA-9602-MS (UC-32), Los Alamos National Laboratory, 1983.

C. J. Josey. General Improvements to the MCNP Alpha-Eigenvalue Solver. Technical Report LA-UR-18-22738, Los Alamos National Laboratory, 2018.

H. G. Kaper. The initial-value transport problem for monoenergetic neutrons in an infinite slab with delayed neutron production. *Journal of Mathematical Analysis and Applications*, 19: 207–230, 1967.

K. Kobayashi. A relation of the coupling coefficient to the eigenvalue separation in the coupled reactors theory. *Annals of Nuclear Energy*, 25:189–201, 1998.

D. Mancusi and A. Zoia. Chaos in eigenvalue search methods. *Annals of Nuclear Energy*, 112: 354–363, 2018.

V. McLane. *Data Formats and Procedures for the Evaluated Nuclear Data File, ENDF-6*. Brookhaven National Laboratory, 2001.

C. B. Moler and G. W. Stewart. An Algorithm for Generalized Matrix Eigenvalue Problems. *Journal on Numerical Analysis*, 10:241–256, 1971.

Y. Nauchi. Attempt to estimate reactor period by natural mode eigenvalue calculation. In *Proceedings of SNA+MC 2013*, Paris, France, 2013.

Y. Nauchi, A. Zoia, and A. Jinaphanh. Analysis of time-eigenvalue and eigenfunctions in the CROCUS benchmark. In *Proceedings of PHYSOR 2020*, Cambridge, United Kingdom, 2020.

K. Nishina and M. Tokashiki. Verification of more general correspondence between eigenvalue separation and coupling coefficient. *Progress in Nuclear Energy*, 30:277–286, 1996.

I. Pázsit and V. Dykin. The role of the eigenvalue separation in reactor dynamics and neutron noise theory. *Journal of Nuclear Science and Technology*, 55(5):484–495, 2018.

R. Y. Rubinstein and D. P. Kroese. *Simulation and the Monte Carlo Method*. J. Wiley and sons, New York, 2007.

R. Sanchez and D. Tomatis. Analysis of alpha modes in multigroup transport. In *Proceedings of the M&C 2019 conference*, Portland, USA, 2019.

A. Santamarina, D. Bernard, P. Blaise, M. Coste, A. Courcelle, T. D. Huynh, C. Jouanne, P. Leconte, O. Litaize, S. Mengelle, G. Noguère, J. M. Ruggiéri, O. Sérot, J. Tommasi, C. Vaglio, and J. F. Vidal. The JEFF-3.1.1 Nuclear Data Library. Technical Report JEFF Report 22, OECD-NEA Data Bank, 2009.

K. P. Singh, S. B. Degweker, R. S. Modak, and K. Singh. Iterative method for obtaining the prompt and the delayed α-modes of the diffusion equation. *Annals of Nuclear Energy*, 38: 1996–2004, 2011.

T. Urbatsch. Fission Matrix Capabilities in MCNP. Technical Report TJU-92-557, Transaction

of the American Nuclear Society, 1992.

I. Variansyah, B. R. Betzler, and W. R. Martin. Multigroup constant calculation with static alpha-eigenvalue monte carlo for time-dependent neutron transport simulations. *Nuclear Science and Engineering*, 194(11):1025–1043, 2020.

G. Velarde, C. Ahnert, and J. M. Aragones. A comparison of the eigenvalue equations in kappa, α, λ and γ in reactor theory. Application to fast and thermal systems in unreflected and reflected configurations. *JEN-392*, 9:49, 1977.

V. Vitali, P. Blaise, F. Chevallier, A. Jinaphanh, and A. Zoia. Spectral analysis by direct and adjoint Monte Carlo methods. *Annals of Nuclear Energy*, 137:107033, 2019.

A. M. Weinberg. Current Status on Nuclear Reactor Theory. *American Journal of Physics*, 20: 401–412, 1952.

T. Yamamoto and H. Sakamoto. Two-step Monte Carlo sensitivity analysis of alpha- and gamma-eigenvalues with the differential operator sampling method. *Annals of Nuclear Energy*, 133: 100–109, 2019.

T. Y. Yamamoto and Y. Nomura. Source Convergence Benchmark 3: Three thick one-dimensional slabs. Technical report, OECD/NEA, 2001.

A. Zoia and E. Brun. Reactor physics analysis of the SPERT III E-core with Tripoli-4®. *Annals of Nuclear Energy*, 90:71–82, 2016.

A. Zoia, E. Brun, and F. Malvagi. Alpha eigenvalue calculations with Tripoli-4®. *Annals of Nuclear Energy*, 63:276–284, 2014.

A. Zoia, E. Brun, F. Damian, and F. Malvagi. Monte Carlo methods for reactor period calculations. *Annals of Nuclear Energy*, 75:627–634, 2015.

A. Zoia, Y. Nauchi, E. Brun, and C. Jouanne. Monte Carlo analysis of the CROCUS benchmark on kinetics parameters calculation. *Annals of Nuclear Energy*, 96:377–388, 2016.